catalysts

MDPI

Article

Optimizing Al and Fe Load during HTC of Water Hyacinth: Improvement of Induced HC Physicochemical Properties

Mara Olivares-Marin [1], Silvia Román [2,*], Beatriz Ledesma [2] and Alfredo Álvarez [3]

[1] Department of Mechanical, Energetic and Materials Engineering, Merida Universitary Center, University of Extremadura, Santa Teresa de Jornet Avenue, 38, 06800 Mérida, Spain
[2] Department of Applied Physics, Industrial Engineering School, University of Extremadura, Elvas Avenue, 06006 Badajoz, Spain
[3] Department of Electrical Engineering, Industrial Engineering School, University of Extremadura, Elvas Avenue, 06006 Badajoz, Spain
* Correspondence: sroman@unex.es; Tel.: +34-924289600

Abstract: Nowadays, several alternatives have been proposed to increase the porosity and/or modify the surface groups of hydrochars from biomasses as well as to develop additional features on them. These alternatives can include specific modifications for the process, as previous steps or as postreatments, and the wide variety of forms in which they can be made can substantially affect the product distribution and properties. In this study, the hydrothermal carbonization process of an invasive floating plant (Water hyacinth) has been modified by introducing different amounts of iron ($FeCl_3$) and aluminium alloy (shaving scrap waste) during the hydrothermal reaction. The effects on process reactivity, phase distribution, and physicochemical properties of the samples obtained were studied by means of different characterization techniques such as thermogravimetry (TG-DTG), physical adsorption/desorption of N_2 at −196 °C, FT-IR spectroscopy, and scanning electron microscopy (SEM). In the case of iron-catalyzed reactions, the magnetite formation and magnetic behavior of the prepared hydrochars after a pyrolytic treatment was also estimated. The results obtained indicate that the porosity of the hydrochars was clearly improved to different extents by the addition of Al or Fe during direct synthesis. In addition, porous carbons with a moderate magnetic character were obtained.

Keywords: hydrothermal carbonization; magnetism; catalyst load; enhancement of porosity

Citation: Olivares-Marin, M.; Román, S.; Ledesma, B.; Álvarez, A. Optimizing Al and Fe Load during HTC of Water Hyacinth: Improvement of Induced HC Physicochemical Properties. *Catalysts* **2023**, *13*, 506. https://doi.org/10.3390/catal13030506

Academic Editor: Michael Renz

Received: 29 December 2022
Revised: 22 February 2023
Accepted: 27 February 2023
Published: 28 February 2023

1. Introduction

Hydrothermal carbonization (HTC) is an exciting valorization technique for converting organic solid waste into valuable products (a solid carbonaceous solid product called hydrochar (HC) and a liquid solution containing many valuable compounds) at relatively low temperatures (150–250 °C) and autogenous pressure [1]. HC can be compared to the char obtained by pyrolysis, because it is a coal-like material with incipient porosity. However, both techniques differ in several aspects, such as energy involved, need of water or activating agent, and properties of liquid phase. In relation to the carbon material, one important difference between a char and a HC is that in general, the former has cleaner pores, as the high temperatures usually associated with the flow of an inert gas help to remove the volatile content of the precursor, leaving behind an incipient porosity (which can be less or cleaner or have variable pore size depending on operating conditions but is also susceptible to being developed by subsequent activation). Chars obtained by pyrolysis usually have a greater C content than HC (i.e., greater heating value), mainly because more oxygen is removed compared to HTC. In addition, the thermal removal of oxygen functionalities and the aromatization developed in char can contribute to the development of a surface chemistry in which, in general, the electrons are more delocalized, and the number of acidic groups is reduced [2].

In contrast, HTC takes place not in an inert atmosphere but rather in a very reactive one in which water becomes a solvent and hydrolyzes the biomass, giving rise to an acidic system where acids are generated and enhance many different biomass degradation reactions (decarboxylation, demethanation, decarbonylation, etc.) so that HCs are generally highly acidic [1]. In addition, during HTC a significant part of the molecules that are formed at the liquid phase can recombine and yield macromolecules that eventually gather to form microspheres that are adsorbed on the HC [3]. This in turn can partially block porosity and also can contribute to increasing the solid yield, especially if long times are used [4]. To improve the low porosity volume of HCs, these materials are often subjected to postheating steps, sometimes under an inert agent [5] or by physical or chemical activation [6].

As the number of researchers working on HTC increases, the number of studies to better understand the nature of the degradation and recombination processes underlying the formation of primary or secondary HCs and the effect of variables apart from the typical (biomass load, time, and temperature) on the product distribution and properties also increases. One aspect that has recently attracted the attention of scientists is how the presence of mineral matter can affect the HTC process [7,8]. This mineral matter can either be part of the starting material or can be added to the process following diverse methodologies (preaddition to biomass by blending or adsorption and incorporation to process water). Mineral matter has been found to affect the process kinetics, reaction pathways, and heat of reactions as well as physicochemical properties of liquid and HC [8].

The addition of metals to the HTC reaction media as well as the introduction of postreatments such as pyrolysis and activation has been proven to affect the structural properties, elemental composition, and chemical surface functionalities; all these changes aimed to upgrade the solid carbon material towards subsequent applications. For example, HCs to be used as fuels should have low N or S and adequate ash composition [6]; if the material is designed to be used as an adsorbent, the development of specific chemical groups and porosity can be specifically interesting for favoring adsorption selectivity [9]; if the final use of the product is as soil amendment, the capture of certain nutrients on the HC is the aim [10].

Previous research has concluded that adding iron(III) chloride ($FeCl_3$) to a HTC system can be an effective way to incorporate Fe to a biomass HC, as compared to other ways of incorporating this metal such as ferromagnetic fluid and Fe particles. In a previous work, the authors found that almond shell $FeCl_3$-assisted HTC followed by pyrolysis could yield microporous magnetic carbon materials [5]. Other sources of Fe, such as Fe_3O_4 particles, have also been embedded to biomass HCs during hydrothermal treatment, and their presence was positive during further CO_2 activation, enhancing the development of microporosity [11]. Both $FeCl_3$ and Fe_3O_4 not only improved the carbon structure but also conferred the HCs with magnetism, after thermal treatment. Magnetism is a very desirable property in an adsorbent, especially when it is going to be used in aqueous solutions. Removing the activated carbon when it is saturated by just approaching a magnet facilitates management and has attracted scientific research [12].

In relation to the use of Al as a catalyst or porosity enhancement agent during HTC, very few scientific references are found. Al has been usually added in the form of salts, such as $Al_2(SO_4)_3$ [6] and $AlCl_3$ [13]. To the authors' knowledge, Al alloys, as a waste generated in the mining industry (particulate matter), have not been used as an additive in HTC processes before.

Eichhornia crassipes, also known as water hyacinth (WH), has been listed as one of the most dangerous invasive plants in the world. This weed is present in many fluvial areas all over warm places of Africa, Asia, and America and absorbs both nutrients and oxygen from water while also preventing sunlight from reaching the deep into bodies of water, resulting in the death of many living species [14]. In addition, the plant obstructs fishing operations in many areas, affecting their economy, which is very significant in the case of African countries in the vicinity of Victoria Lake, where it has also been associated

with the propagation of plagues. Finally, WH's presence has damaged devices from hydric plants [13]. The challenge of making WH disappear without using chemicals that are toxic to other animals has moved the scientific community to find ways of managing this biomass involving thermal treatment to avoid spore dissemination. In Spain, fighting this weed has become a national priority, as is the case also in many other areas of the world, and the solution does not seem to be easy because it is extremely resistant (seeds can live for more than 20 years), has a very high growing rate, and can reproduce and spread very quickly [15]. In the basin of Guadiana River in southwest Spain, EUR 50 million was spent between 2004 and 2020 where WH had expanded over a length of 185 km along the river (total perimeter affected = 630 km) [16].

In this study, the use of this novel precursor (WH) has been investigated to produce, by Al- and Fe-catalyzed HTC, porous carbon materials. In both cases, for the first time how the catalyst load can affect process reactivity and structural and chemical changes of HCs and, in the case of Fe-assisted processes, additional potential magnetization due to further pyrolysis of the HCs was evaluated.

2. Results

2.1. Reactivity of Processes

Tables 1 and 2 display the solid yield values (SY, %) obtained for uncatalyzed Fe and Al-catalyzed HTC experiments. These results can be better analyzed in the precursor biomass degradation analyses that have been plotted in Figure 1.

Table 1. Solid yield (SY, %) and N_2 adsorption textural parameters of uncatalyzed HC and Al-catalyzed HCs.

	Solid Yield (%)	S_{BET}, m^2g^{-1}	V_{mi}, cm^3g^{-1}	V_{me}, cm^3g^{-1}	V_T, cm^3g^{-1}	S_{ext}, m^2g^{-1}
WH-HC	26.8	23	0.005	0.019	0.024	26
WH-HC-Al5	20.6	38	0.005	0.023	0.028	42
WH-HC-Al10	28.6	35	0.005	0.033	0.038	39
WH-HC-Al20	27.0	49	0.010	0.045	0.055	53

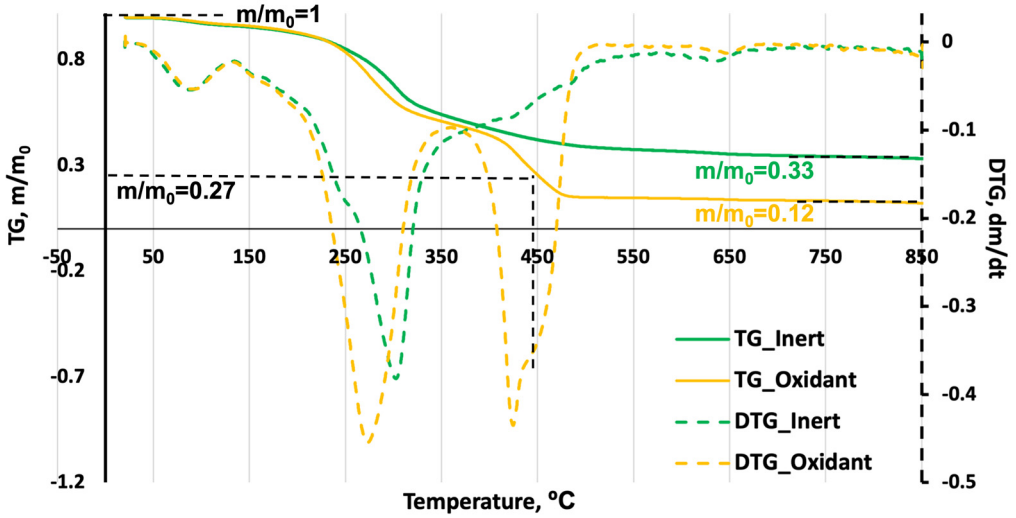

Figure 1. TGA and DTG curves of WH leaves under inert and oxidant atmosphere.

According to thermogravimetric analysis (TGA), under pyrolytic conditions, WH degrades mainly in the range 240–400 °C, with a residual degradation prevailing up to 550 °C and a very slight mass loss up to 850 °C (fixed carbon plus ash content can be estimated as residual mass at this temperature, that is, around 33%). When air is used as carrier gas, the degradation profiles change significantly; at the TGA curve, there are several slopes with two main significant degradation rates in the temperature ranges: 244–320 °C (this is close to the inert analysis) and 390–472 °C (here, the degradation behavior clearly differs from inert analyses). In fact, after this drop the WH residual mass reaches a value that is similar to the one found for HTC (26.8%). Final residual mass percentage upon combustion is 12%.

This suggests that HTC under the conditions here studied represents a middle situation between pyrolysis and combustion. This is consistent with the fact that volatile matter (most of it) was degraded during HTC, but additional reactions removed a part of the biomass that was resistant to pyrolysis because of the joint effect of water under subcritical conditions (H_3O^+) and many reactive molecules resulting from hemicellulose and cellulose degradation (mainly organic and inorganic acids). The presence of such molecules makes the system highly reactive and, as a whole, involve a complex combination of many types of degradation reactions (dehydration, decarboxylation, demethanation, decarbonylation, etc.) [1]. Other biomass materials (including water hyacinth stem and many lignocellulosic precursors) have given, under the same temperature, time, load, and reactor conditions, greater values of HTC solid yield [17].

2.2. Aluminium-Catalyzed HTC

Figure 2 shows the adsorption/desorption isotherms of the HCs obtained from uncatalyzed and Al-catalyzed WH leaves through HTC, while typical porosity parameters have been included in Table 1. According to these results, the addition of the Al alloy during HTC caused a slight change on the porous structure of the HCs. In the first place, the uncatalyzed process, as expected from most previously published studies on HTC, does not yield a carbon material with noticeable porosity development (S_{BET} of 23 m^2g^{-1}, with an almost negligible contribution of microporosity because of pore blockage by adsorbed, condensed, or polymerized biomass fragments) [1]. The addition of Al resulted in a slight improvement in porosity, which was more significant with the addition of a greater amount of metal (20 g) during HTC. The rise in N_2 adsorption at greater relative pressure values (Figure 2) suggest that Al was specifically effective in opening mesopores and external areas; total pore volume (V_T) was almost doubled by adding 20 g of Al, as compared to the pristine HC (0.055 vs. 0.024 cm^3g^{-1}). In fact, if one focuses on the lower relative pressure zone, it can be observed that the increase in N_2 adsorption is more abrupt for the noncatalyzed sample.

Other aluminum compounds, such as $AlCl_3$, added during the HTC of other biomass materials have also been effective in opening micropores, yielding mesoporous materials, with N_2 adsorption isotherms growing along the whole range of relative pressure, as is reported in the work of Liu et al. [13]. These authors, however, subjected the materials to subsequent aerobic calcination to favor the formation of Al-oxide active sites.

Al in the liquid phase under subcritical conditions has been reported to be converted into hydroxide ($2Al + 6H_2O \rightarrow 2Al(OH)_3 + 3H_2$), which in turn might have catalyzed the hydrogasification of the HC amorphous surface carbon ($C + 2H_2 \rightarrow CH_4$) [18].

Surface chemical functionalities, as determined by FT-IR spectrometry, suggested that the hydrothermal process involved the breaking up of cellulose and hemicellulose (compare signals of WH leaves, uncatalyzed HC, and HCs obtained using different amount of Al during HTC, plotted in Figure 3). Assignation of bands was based on previous studies [19].

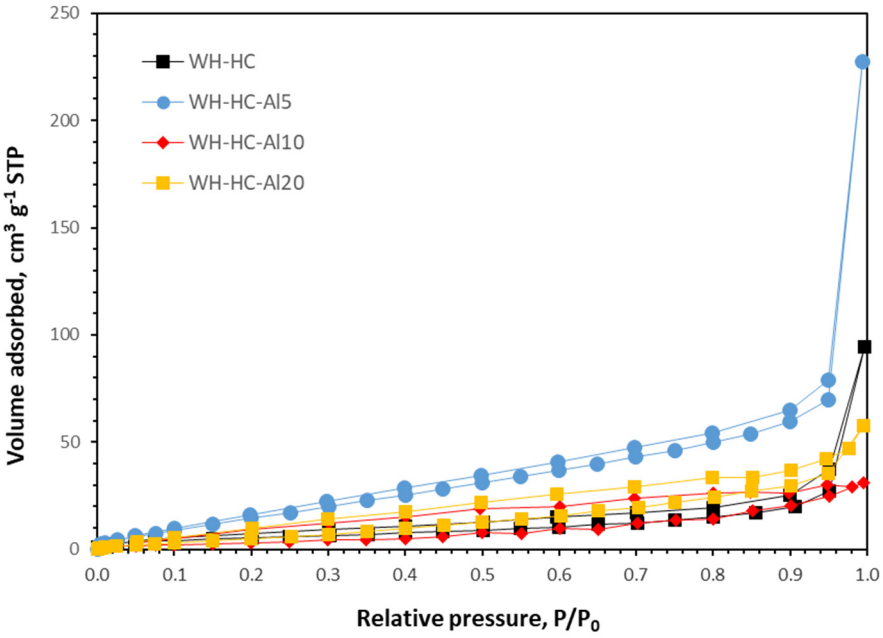

Figure 2. N_2 adsorption/desorption isotherms at −196 °C of uncatalyzed HC and HCs prepared by Al-catalyzed HCs.

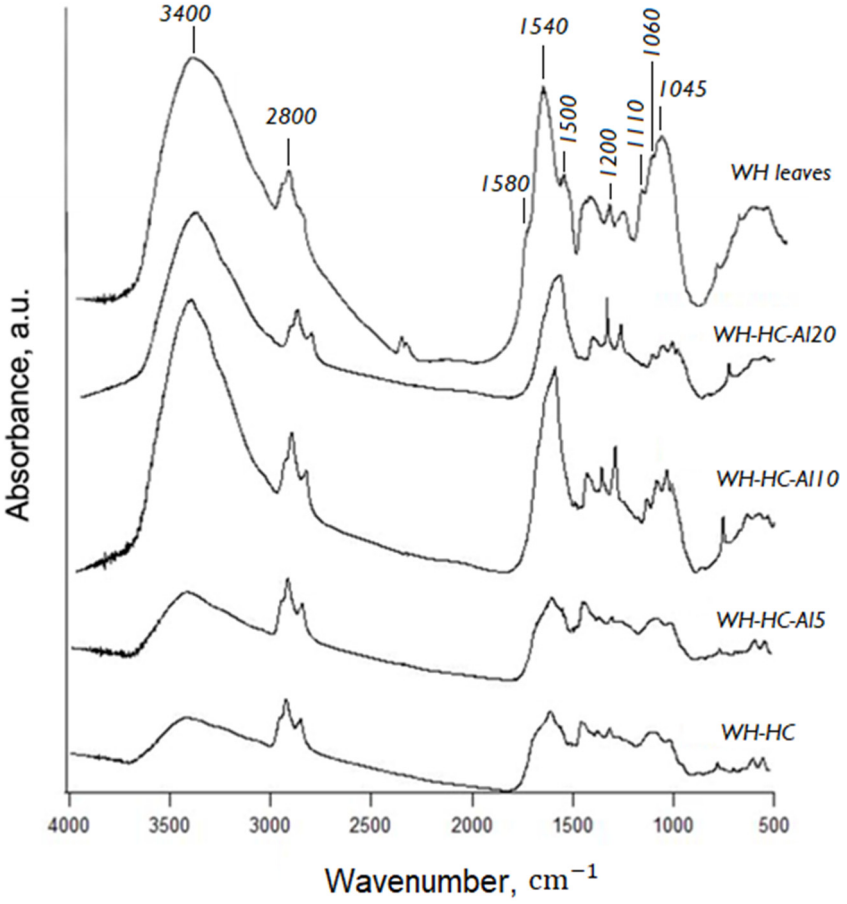

Figure 3. FT-IR spectra of WH, uncatalyzed HC and HCs prepared by Al-assisted HTC.

For instance, the loss of cellulose-type spectral bands at the pristine precursor are removed after HTC; that is the case of C-O bonds in alcohols of pyranose rings 1110, 1060, and 1045 cm^{-1} (see Figure 3). Moreover, the signals at wave numbers in the range

1600–1500 cm^{-1} found for hydrothermal-treated samples (and not for WH leaves) can be assigned to C=O vibrations on olefinic and/or aromatic structures, as also happens for C-O vibrations, typical for eter structures (1200 cm^{-1}), that are only visible for HCs.

The addition of Al alloy under these conditions to the reaction medium do not have a remarkable effect on the number, intensity, and position of the spectral bands of the HCs under any concentration, as compared to the uncatalyzed HTC run.

SEM analyses (Figure 4) revealed that the presence of Al alloy on the liquid–solid system altered the surface morphology of the HCs. In the case of the uncatalyzed reaction (WH-HC), the surface is full of pleats, with a low opening of pores and the presence of some microspheres. Other research [17] made under similar uncatalyzed HTC conditions have shown greater abundancy of these spheres; this might indicate that condensation reactions were less prominent in the present case or that their deposition on the primary HC was less facilitated because of diffusion of electrostatic resistance.

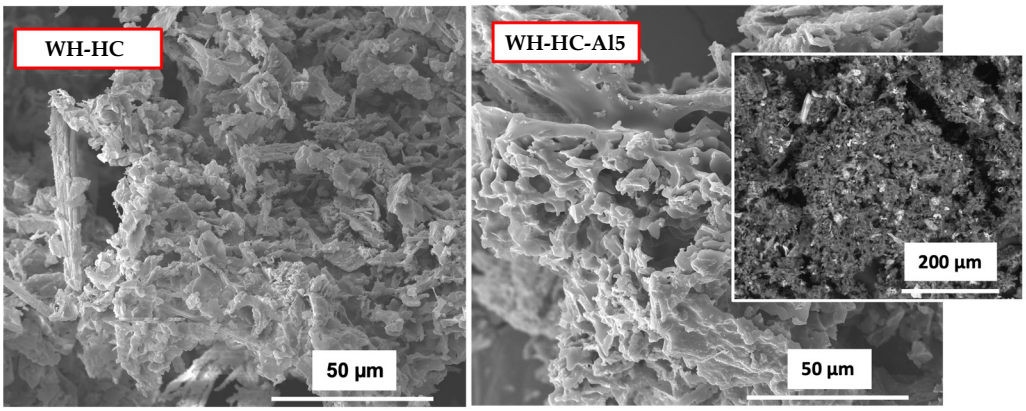

Figure 4. SEM micrographs of uncatalyzed HC and WH-HC-Al5. Embebed image on the right is a retro-dispersed electron image of WH-HC-Al5.

The images obtained with the retro-dispersed electron detector show small bright particles of different size and shape heterogeneously incorporated on the carbon matrix (see image inserted on the right in Figure 4). EDAX quantification analyses of the WH-HC-Al5 particles showed that apart from carbon (62.0%, wt./wt.) and oxygen (22.6%), metals such as calcium (1.5%), aluminum (1.7%), and phosphorous (0.9%) were present in the material.

2.3. Iron-Catalyzed HTC

Table 2 lists the SY values (both after HTC, SY, and after subsequent pyrolysis, WSY) as well as HC typical porosity features, as determined from N_2 adsorption isotherms at −196 °C (plotted in Figure 5). The addition of Fe and the further thermal treatment resulted in a greater reactivity and lower SY in relation to the uncatalyzed run except for the experiment made under the lowest Fe concentration (WH-HC-Fe0.25-600), which showed a rise in SY.

Table 2. Solid yield (SY, %) and N_2 adsorption textural parameters of Fe-catalyzed HTC.

	SY (%)	WSY (%)	S_{BET}, m^2g^{-1}	V_{mi}, cm^3g^{-1}	V_{me}, cm^3g^{-1}	V_T, cm^3g^{-1}	S_{ext}, m^2g^{-1}
WH-HC	26.8	-	23	0.005	0.019	0.024	33
WH-HC-Fe0.25-600	33.2	13.73	229	0.101	0.099	0.200	80
WH-HC-Fe0.5-600	22.3	11.15	76	0.023	0.075	0.098	78
WH-HC-Fe0.75-600	22.7	11.55	66	0.018	0.054	0.072	69

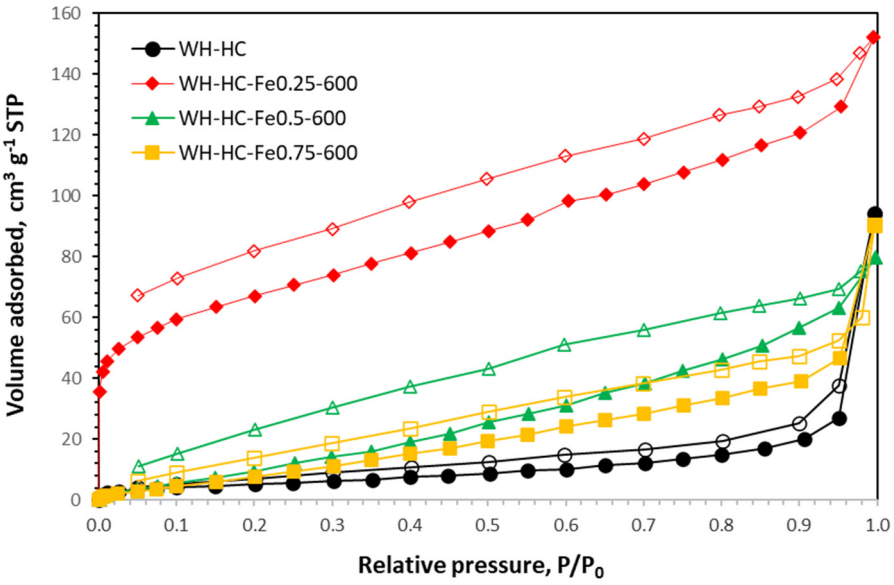

Figure 5. N_2 adsorption isotherms at −196 °C of WH-HC and HCs prepared by Fe-assisted HTC.

Increasing the $FeCl_3$ solution molarity might help bond breakage, as has been suggested in the specific case of cellulose [20], and could also inhibit adsorption of secondary HC that could be related to mass and energy transference resistance under such high concentrations.

A significantly better porosity improvement was found for Fe-catalyzed reactions in relation to Al-catalyzed samples. An apparent surface rise was found for the sample obtained at the lowest Fe concentration (0.25 M). In this way, the first point at the lowest relative pressure is much higher for sample WH-HC-Fe0.25-600, indicating a high contribution of primary micropores; this sample, however, also presents mesopores, as the N_2 gradually increases along the whole range of relative pressure.

Increasing metal concentration over 0.25 M is detrimental to pore development; not only do these samples have lower pore volumes, but their pore size distribution is also wider and larger. This result, joined to the lower SY found for samples made at 0.5 and 0.75 M, might indicate that pore destruction is taking place under such conditions (external burning could be postulated or maybe disorganized carbon removal could be inhibited under these conditions, taking into consideration that isotherms for these two runs are type III).

According to X. Zhu et al. [20], during pyrolysis, Fe^{3+} ions are hydrolyzed to amorphous Fe species ($Fe(OH)_3$ and FeO(OH)) at temperatures lower than 350 °C. Subsequently, these species are converted into Fe_2O_3 at temperatures lower than 400 °C. At higher temperatures (500–700 °C), Fe_2O_3 should be reduced to Fe_3O_4 with the aim of reducing components such as amorphous carbon and gaseous CO. Finally, both Fe_2O_3 and Fe_3O_4 with the amorphous carbon yield the metal Fe.

Figure 6 shows a particle of sample WH-HC-Fe0.25-600. One can clearly see the homogeneously distributed particles on the carbon structure of the HC, whose EDX analyses confirm that they consist of Fe (this metal was with difference the most abundant, with a contribution of 9.3% wt./wt., being the proportion of C and O equal to 80.0 and 9.2, respectively). The image also allows identifying slit-shaped open pores that developped after the calcination process. Hao et al. [11] found both effects when hydrothermally treating several biomass materials to Fe_3O_4 (during HTC) and further CO_2 activation.

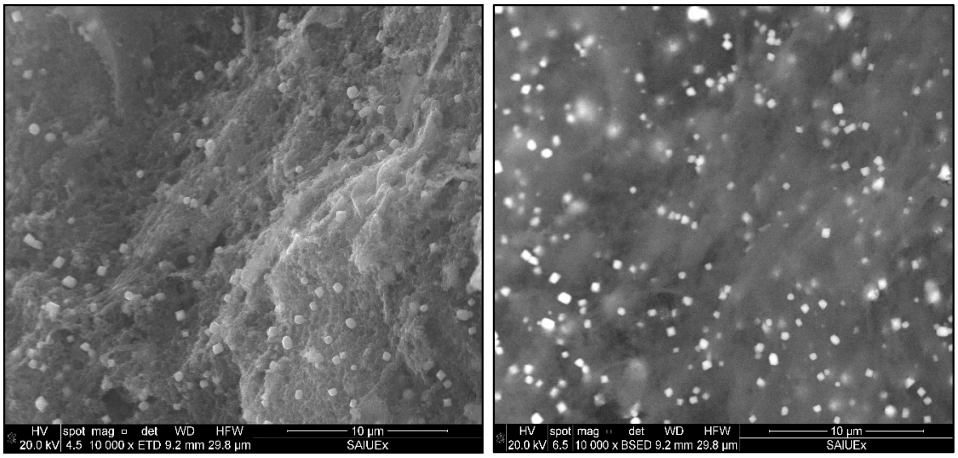

Figure 6. SEM micrographs of WH-HC-Fe0.25-600 (**left**) and its respective retro-dispersed electron image (**right**).

The FT-IR surface chemistry analysis made on the HCs have been included in Figure 7. As expected, the pyrolytic stage involved the removal of a significant quantity of the HC functional groups due to the high temperature applied. At the same time, these bonds suggest that the aromatization of the surface was intensified. In general, the three spectra are very similar, and the bands at 1600 y 1200 cm^{-1} typical of C=C bonds in aromatic rings and C-O in alcohols, ethers, or esters can be highlighted [19].

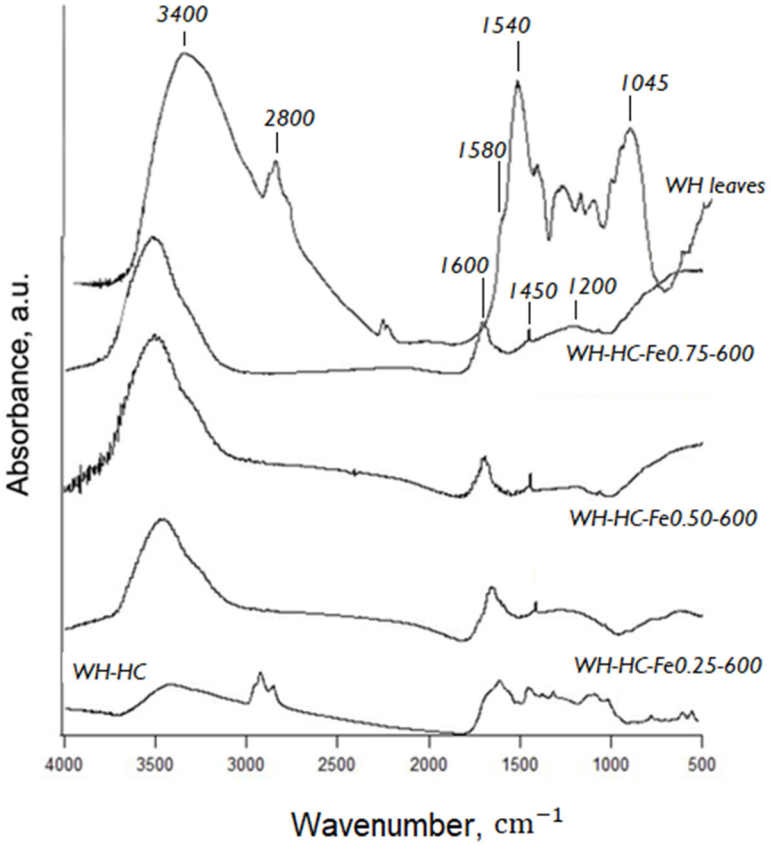

Figure 7. FT-IR spectra of WH, WH-HC, HCs, and HCs prepared by Fe-assisted HTC.

2.4. Magnetic Measurements

The magnetic behavior of the HCs prepared by Fe-assisted HTC was measured using a homemade installation (see details and equations employed in Section 3.3.3). This setup

allowed the determination of magnetic susceptibility (X_m) of samples. Magnetization curves of Fe-catalyzed samples under a current of 8.5 A have been plotted in Figure 8.

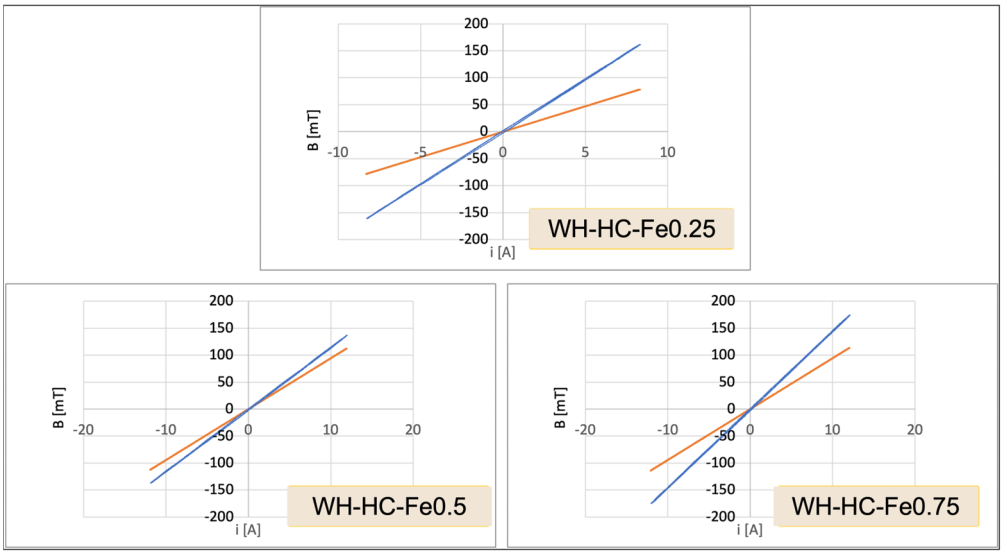

Figure 8. Magnetization curves applied to Fe-catalyzed HCs.

A correlation was found between the values of magnetic susceptibility found for the HCs and the porous development that was created upon the hydrothermal plus pyrolytic stage. In this way, the sample made using an $FeCl_3$ concentration of 0.25 M that showed the highest S_{BET} (229 m^2/g) also gave the greatest X_m (1.048). This value was much higher than that found for almond shell HCs obtained under the same reaction conditions and same installation (0.514), as reported in a previous work [9]. In that study, the authors found better results if pyrolysis was made at 800 °C than at 600 °C; however, for WH, making runs at 800 °C resulted not only in a porosity destruction but also in a significant drop of X_m (these results have not been shown here for the sake of brevity). These findings demonstrate that general assumptions cannot be made, and each biomass precursor must be specifically studied.

The other two samples made in this study, WH-HC-Fe0.5 and WH-HC-Fe0.75 that had a very poor and a similar pore volume, respectively, showed much lower values of X_m (0.27 and 0.46, respectively, under the same conditions).

3. Materials and Methods

3.1. Materials

Water hyacinth (WH) was gathered from the Guadiana River basin at Badajoz (southwest Spain, GPS coordinates 38.883889, −6.976824). The weed was pulled up and carried in hermetic plastic 15 L drums, and the three main parts (leaves, stem, and roots) were manually separated. Only leaves were used in this study because of their most favorable carbon density. After being oven-dried (110 °C, 12 h), WH leaves were crushed and sieved to a particle size of 1–2 mm (CISA 200/50 sieve, Norm ISO-3310.1); the particle size was chosen based on previous research with other lignocellulosic materials to guarantee that obtained HCs would have a granular character. The elemental analysis of the dried biomass showed proportions of C, O, H, and N equal to 41.14%, 4.93%, 49.63%, and 4.16%, respectively.

Aluminum alloy (AA2011 alloy) scraws were supplied from a local mining factory, as waste from their operation, in the form of particles with sizes of 2–4 mm. $FeCl_3$ was used in the form of iron (III) chloride 6-hydrate, as purchased from Panreac Applichem (Barcelona, Spain).

3.2. Methods

3.2.1. Standard HTC Processes

The standard HTC processes were performed in a 0.2 stainless steel autoclave (Berghof, Berlin, Germany) provided with a Teflon vessel. The dried biomass (10 g) was added to 150 mL of tap water, and the solution was kept under stirring conditions for 1 h. Thereafter, it was transferred to the Teflon vessel and introduced on the autoclave, which was then placed into a preheated oven (230 °C). The total time from the moment it was introduced in the oven and taken out was 20 h; this time period has been chosen based on previous experience of the research group [17], which demonstrated that this dwell time is enough to guarantee reaching a solid yield plateau that, in turn, indicates that biomass degradation for those temperature conditions is guaranteed. When the reaction time was reached, the autoclave was removed from the oven and subsequently placed in a cold-water bath and allowed to cool to room temperature.

After cooling, the solid phase was separated from the liquid by vacuum filtration and subsequently dried at 80 °C to remove residual moisture. The dried HC was stored in closed flasks that were placed into a desiccator until further analysis. The experiments were carried out under autogenous pressure in an autoclave without the possibility of measuring interior conditions, but according to previous studies, the pressure inside the vessel equaled that of the water at saturated conditions.

3.2.2. Modified Hydrothermal Carbonization Processes

For aluminum-catalyzed hydrothermal processes, a prefixed amount of Al particles (5, 10, or 20 g) was added to the water–biomass solution (100 mL of water and 3 g of CAM; that is, Al to biomass ratio of 5:3, 10:3, and 20:3) and subjected to HTC as in the case of the standard reaction. After filtrating the slurry, containing both the metal particles and the HC, the former was manually separated with the aim of pliers, and only HC weight accounted for SY.

These samples were named according to the nomenclature WH-HC-AlX, where X represents the amount of metal added to the system (for instance, WH-HC-Al5 stands for a sample in which 5 g of Al was added to HTC).

In the case of the processes catalyzed with iron, an Fe-containing mixture ($FeCl_3 \cdot 6H_2O$) of different concentration (0.25 M, 0.5 M and 0.75 M) was added (50 mL) to the dried weed (3 g) and directly subjected to HTC. These samples were named according to the nomenclature WH-HC-FeX-600, where X represents the amount of metal added to the system (for instance, WH-HC-Fe0.25-600 stands for a sample in which the concentration of $FeCl_3 \cdot 6H_2O$ mixture added to HTC was 0.25 M).

Then, Fe-catalyzed HCs were subjected to pyrolysis at 600 °C (N_2, 100 mL min^{-1}) in a vertical stainless steel piece of equipment described elsewhere [21].

3.3. Characterization Techniques

3.3.1. HC Reactivity and Thermal Behavior

Solid yield (SY, %) was calculated as the amount of solid product (i.e., HC) obtained after HTC in relation to the initial mass of precursor, expressed in percentage. For those runs catalyzed with Fe in which a second pyrolysis step was required, the whole solid yield (WSY) was calculated by considering both yield; that is, both fractions values were multiplied. In this way, the SY represents the final mass of char after HTC and pyrolysis in relation to the initial biomass mass.

Thermal analyses (TGA and DTG), were performed using a thermobalance (Setsys Evolution Setaram, Madrid, Spain). Argon or air (100 mL min^{-1} in both cases) were used as carrier agents, and a heating rate of 10 °C min^{-1} was applied.

3.3.2. HC Porosity and Surface Chemistry

The porosity of the HCs was explored by N_2 adsorption/desorption at −196 °C using a semiautomatic adsorption unit (AUTOSORB-1, Quantachrome, Tallahassee, FL,

USA). Prior to analyses, the samples were outgassed at 120 °C for 12 h. Experimental adsorption data were analyzed using suitable methods [22] to calculate (a) the value of the BET-specific surface (S_{BET}); (b) the external surface (S_{EXT}), calculated by the α_s method, using the reference nonporous solid proposed by Carrott et al. [23]; (c) the percentage of internal surface (S_{INT}), calculated as the difference between S_{BET} and S_{EXT}; (d) the volume of micropores through the Dubinin–Radushkevich equation (V_{miDR}); and (e) the volume of mesopores (V_{me}), calculated as the difference between the pore volume at p/p0 = 0.95 and p/p0 = 0.10.

In addition, the surface morphology of the samples was analyzed by scanning electron micrography (SEM, Hitachi, S-3600N, Krefeld, Germany) observation. The SEM samples were prepared by depositing about 50 mg of sample on an aluminum stud covered with conductive adhesive carbon tape and then coating with Rd–Pd for 1 min to prevent charging during observations. Imaging was done in the high vacuum mode at an accelerating voltage of 20 kV using secondary electrons.

Finally, the surface chemistry of the HCs was evaluated by means of FTIR spectroscopy. FTIR spectra were recorded with a Perkin Elmer model Paragon 1000PC spectrophotometer (Waltham, MA, USA) using the KBr disc method, with a resolution of 4 cm^{-1} and 100 scans (Perkin–Elmer 1720, Waltham, MA, USA). The composition of the cristaline part of the HCs was also analyzed by X-ray diffraction using Bruker equipment (Warwick, RI, USA).

3.3.3. Experimental Setup for the Study of Magnetic Behavior

The equipment used to measure the magnetic performance of materials has been described elsewhere [5]. Briefly, the HC was introduced on a cylindrical plastic tube (0.005 m diameter), a copper coil was wound 100 turns to be used as a pickup coil. The sample was then placed in the center of a long excitation coil (at the central part, far away from the ends) and subjected to external AC magnetic fields, H, created by different currents.

Under these conditions, H is quite uniform in the sample and can be written as

$$H = ni_{ex} \tag{1}$$

where n is the number of turns per meter of the excitation coil, that is,

$$n = \frac{N_{ex}}{L}. \tag{2}$$

in which L is the length of the coil.

As is known, the magnetic susceptibility is

$$\chi_m = \frac{1}{\mu_0 H}(B_{HC} - B_0) \tag{3}$$

where m_0 is the vacuum permeability (4p $\times$ 10^{-7} H/m) and B_{HC} and B_0 are the magnetic flux density in the sample and the air, respectively.

In order to determine the flux densities, two measurements are carried out as shown in Figure 9:

The *fem* measured in Figure 9 (leftside image) permits us to find B_{HC} by applicating the Faraday's law,

$$B_{HC} = -\frac{1}{N_{pu}S}\int emf\, dt \tag{4}$$

where S is the cross section of the sample, approximately equal to that of the pickup coil, and N_{HC} is the pickup coil number of turns.

The magnetic flux density measured by the Hall probe in Figure 9 (right-side image) is B_0. Substituting this value and the result of Equation (4) in Equation (3), magnetic susceptibility can be obtained.

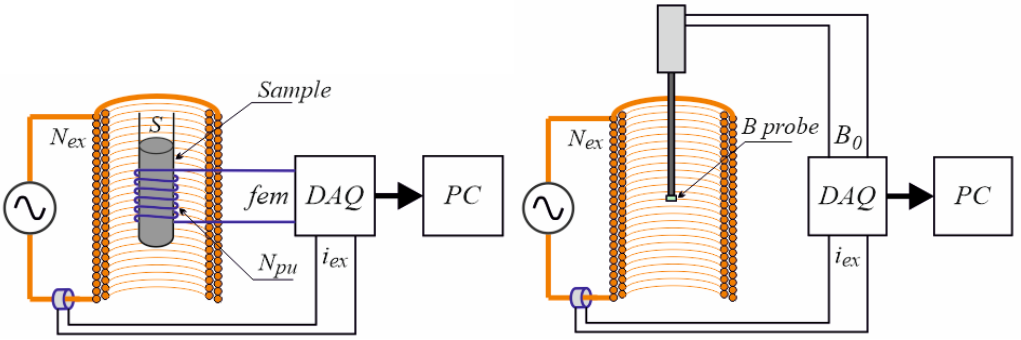

Figure 9. Setups to determine the magnetic susceptibility of carbons as B_{HC} (**left**) and B_0 (**right**).

4. Conclusions

Water hyacinth leaf HTC can yield a carbon material whose porosity is susceptible to being improved by means of the addition of Al or Fe to the reaction medium, although to a different extent. While Al addition induced a little porosity development and a slight widening of microporosity for smaller quantities of catalyst, the total pore volume was almost doubled in reference to the uncatalyzed HTC run (without further thermal treatment); the best result was found when the largest amount of Al alloy (20 g) was added to the system.

On the other hand, Fe, added as $FeCl_3$, clearly was more beneficial when a lower mixture concentration was used; for this metal, a concentration of 0.25 M yielded a carbon with a S_{BET} of 229 m^2/g, about 100 times higher than the noncatalyzed run. In this reaction, the use of a further pyrolytic step not only improved the HC activation but also induced a magnetic character to the carbon particles (magnetic susceptibility of 1.048) that could be easily isolated from their fluid medium by application of a magnetic field.

Author Contributions: Conceptualization, M.O.-M.; methodology, S.R., B.L. and A.Á.; validation, M.O.-M. and A.Á.; formal analysis, M.O.-M. and S.R.; investigation, B.L. and A.Á.; resources, M.O.-M. and S.R.; writing—original draft preparation, S.R. and A.Á.; writing—review and editing, M.O.-M.; funding acquisition, S.R. and M.O.-M. All authors have read and agreed to the published version of the manuscript.

Funding: This research was funded by the Agencia Estatal de Investigación (MINCIN), grant number PID2020-116144RB-I00/AEI/10.13039/501100011033XXX.

Acknowledgments: The authors thank the SAIUEX (Servicios de Apoyo a la Investigación de la Universidad de Extremadura) for support during the porosimetry characterization of carbon materials.

Conflicts of Interest: The authors declare no conflict of interest. The funders had no role in the design of the study; in the collection, analyses, or interpretation of data; in the writing of the manuscript; or in the decision to publish the results.

References

1. Román, S.; Libra, J.; Berge, N.; Sabio, E.; Ro, K.; Li, L.; Ledesma, B.; Álvarez, A.; Bae, S. Hydrothermal Carbonization: Modeling, Final Properties Design and Applications: A Review. *Energies* **2018**, *11*, 216. [CrossRef]
2. Moreno-Castilla, C.; López-Ramón, M.V.; Carrasco-Marín, F. Changes in surface chemistry ofactivated carbons by wet oxidation. *Carbon* **2000**, *38*, 1995–2001. [CrossRef]
3. Sevilla, M.; Fuertes, A.B. The production of carbon materials by hydrothermal carbonization of cellulose. *Carbon* **2009**, *47*, 2281–2289. [CrossRef]
4. Jung, D.; Zimmermann, M.; Kruse, A. Hydrothermal carbonization of fructose: Growth mechanisms and kinetic model. *ACS Sustain. Chem. Eng.* **2018**, *6*, 13877. [CrossRef]
5. Olivares, M.; Román, S.; Ledesma, B.; Álvarez, A. Magnetic Behavior of Carbon Materials Made from Biomass by Fe-Assisted Hydrothermal Carbonization. *Molecules* **2019**, *24*, 3996. [CrossRef]
6. Haj Yahia, S.; Lee, K.K.; Ayed, B.; Heddin, N.; Church, T.L. Activated Carbons from Hydrochars Prepared in Milk. *Sci. Rep.* **2019**, *9*, 16956. [CrossRef] [PubMed]
7. Mäkelä, M.; Fullana, A.; Yoshikawa, K. Ash behavior during hydrothermal treatment for solid fuel applications. Part 1: Overview of different feedstock. *Energy Convers. Manag.* **2016**, *121*, 402–408. [CrossRef]

8. Hammerton, J.M.; Ross, A.B. Inorganic Salt Catalysed Hydrothermal Carbonisation (HTC) of Cellulose. *Catalysts* **2022**, *12*, 492. [CrossRef]
9. Román, S.; Valente Nabais, J.M.; Ledesma, B.; Laginhas, C.; Titirici, M.-M. Surface Interactions during the Removal of Emerging Contaminants by Hydrochar-Based Adsorbents. *Molecules* **2020**, *25*, 2264. [CrossRef] [PubMed]
10. Chen, Y.; Sun, Z.; Su, Y.; Yang, J.; Li, M.; Hong, B.; Chen, G. Hydrochar Derived from Spent Mushroom Substrate Ameliorates Soil Properties and Nutrient Levels in Saline–Sodic Soil: An Incubation Study. *Sustainability* **2022**, *14*, 12958. [CrossRef]
11. Hao, W.; Björkman, E.; Yun, Y.; Lilliestråle, M.; Hedin, N. Iron Oxide Nanoparticles Embedded in Activated Carbons Prepared from Hydrothermally Treated Waste Biomass. *ChemSusChem* **2014**, *7*, 875. [CrossRef] [PubMed]
12. Phouthavong, V.; Yan, R.; Nijpanich, S.; Hagio, T.; Ichino, R.; Kong, L.; Li, L. Magnetic Adsorbents for Wastewater Treatment: Advancements in Their Synthesis Methods. *Materials* **2022**, *15*, 1053. [CrossRef] [PubMed]
13. Liu, J.; Yang, L.; Shuang, E.; Jin, C.; Gong, C.; Sheng, K.; Zhang, X. Facile one-pot synthesis of functional hydrochar catalyst for biomass valorization. *Fuel* **2022**, *315*, 123172–123183. [CrossRef]
14. NASA Reports. Earth Observatory: Water Hyacinth Re-Invades Lake Victoria. Available online: https://earthobservatory.nasa.gov/images/7426/water-hyacinth-re-invades-lake-victoria (accessed on 10 February 2023).
15. García-De-Lomas, J.; Dana, E.; Borrero, J.; Yuste, J.; Corpas, A.; Boniquito, J.; Castilleja, F.; Martínez, J.; Rodríguez, C.; Verloove, F. Rapid response to water hyacinth (Eichhornia crassipes) invasion in the Guadalquivir river branch in Seville (southern Spain). *Manag. Biol. Invasions* **2022**, *13*, 724–736. [CrossRef]
16. MITECO. Available online: https://www.miteco.gob.es/es/prensa/ultimas-noticias/el-camalote-est%C3%A1-controlado-en-todos-los-tramos-del-r%C3%ADo-guadiana/tcm:30-520159 (accessed on 10 February 2023).
17. Román, S.; Ledesma, B.; Álvarez, A.; Coronella, C.; Qaramaleki, S.V. Suitability of hydrothermal carbonization to convert water hyacinth to added-value products. *Renew. Energy* **2020**, *146*, 1649–1658. [CrossRef]
18. Shmelev, V.; Nikolaev, V.; Lee, J.H.; Yim, C. Hydrogen production by reaction of aluminum with water. *Int. J. Hydrogen Energy* **2016**, *41*, 16664. [CrossRef]
19. Fanning, P.E.; Vannice, M.A. A DRIFTS study of the formation of surface groups on carbon by oxidation. *Carbon* **1993**, *31*, 721–730. [CrossRef]
20. Zhu, X.; Qian, F.; Liu, Y.; Matera, D.; Wu, G.; Zhang, S.; Chen, J. Controllable synthesis of magnetic carbon composites with high porosity and strong acid resistance from hydrochar for efficient removal of organic pollutants: An overlooked influence. *Carbon* **2016**, *99*, 338–347. [CrossRef]
21. González, J.F.; Encinar, J.M.; Canito, J.L.; Sabio, E.; Chacón, M. Pyrolysis of cherry stones: Energy uses of the different fractions and kinetic study. *J. Anal. Appl. Pyrolysis* **2003**, *67*, 165–190. [CrossRef]
22. Sing, K.S.W.; Everett, D.H.; Haul, R.A.W.; Moscou, L.; Pierotti, R.A.; Siemieinewska, T. Reporting physisorption data for gas/solid systems with special reference to the determination of surface area and porosity. *Pure Appl. Chem.* **1985**, *57*, 613–619. [CrossRef]
23. Carrott, P.J.M.; Roberts, R.A.; Sing, K.S.W. Standard nitrogen adsorption data for nonporous carbons. *Carbon* **1987**, *25*, 769–770. [CrossRef]